Soils and Rocks
www.soilsandrocks.com
An International Journal of Geotechnical and Geoenvironmental Engineering
ISSN 1980-9743
ISSN-e 2675-5475

The 2022 Pacheco Silva lecture: The influence of residual loads on pile foundation behavior

Bernadete Ragoni Danziger[1#]

Lecture

Keywords
Residual loads
Load transfer
Settlement prediction
Pile stiffness

Abstract

Residual loads can affect the load transfer and the settlement-induced in-service loadings, although they do not alter the bearing capacity. When residual loads are present and not measured or evaluated, the settlement estimate is greater than predicted if these loads are known. Residual loads can be measured when the pile instrumentation is nullified before pile installation, in the case of displacement piles, or before the first loading in non-displacement piles, such as bored cast-in-place piles, continuous flight auger piles, and micro-piles. In the case of underpinning foundation and piled raft, when the loading transfer is shared by the original and new foundation, or by the piles and the raft, it is essential to know the stiffness of each foundation element to estimate the load partition. If residual loads are present, pile stiffness is greater than when not considered in the design. The paper revisits this theme of practical relevance. A historical review of the most relevant research involving pile residual load measurements, pile loading tests including the interpretation of residual loads locked at a pile toe, and a new procedure for residual loads prediction are provided. A comparison is made of the experimental residual loads observed in some of the instrumented cases and the values estimated with the suggested procedure. The development of residual loads at the pile toe as a function of the toe resistance to total capacity ratio is very similar to the variation of the soil density as a function of soil moisture content in soil compaction.

1. Introduction

When a pile is unloaded after undergoing compression, its shaft tends to return to its original length. The surrounding soil mass restricts the complete shaft unloading and causes negative friction at the pile shaft close to ground level, which is equilibrated by the positive skin friction and the residual load at the pile toe. The pile is loaded even when no force is applied to its top, as shown in Figure 1a. The pile is pre-compressed. The neutral plane is at the elevation where the compressive residual load is maximum, and the shear stress is zero. Until the pile undergoes a greater top load than the maximum residual load, the shear resistance is reversed, and negative friction is completely nullified with a very insignificant load transferred to the shaft below the neutral plane and the pile toe. Only with an additional load applied to the pile top can the settlement at the pile toe be felt in a relevant mode, as illustrated in Figure 1b.

Residual loads are the loads locked at the pile shaft and pile toe after unloading, due to driving or static or dynamic tests, as indicated in Figure 1a.

When an instrumented pile is loaded to failure and the transfer load is observed during the test, two distinct curves can result, as shown in Figure 2. In this figure, the instruments may be zeroed at different times. In Figure 2a on the left, the true load transfer is obtained when the instruments are zeroed before driving (or before the first loading of a non-displacement pile in a static loading test). In Figure 2b on the right, the false load transfer is obtained in a test when the instruments are zeroed after driving, or after a previous loading in a test.

The true load transfer in Figure 2a captures the residual load locked into the pile shaft and toe after driving, and the additional load mobilized by the soil at pile lateral contact and at the pile toe. From the transferred true load at failure, it is possible to separate the total mobilized resistance at failure by lateral soil resistance, $Q_{l,rupt}$, from that available by the total point resistance, $Q_{p,rupt}$. The false toad transfer obtained in Figure 2b is the residual loads already present after driving (or after the previous loading) subtracted from the total true load. Only this difference is captured by the instruments zeroed after driving or after the previous loading. It is clearly noticeable in Figure 2b that the transfer curve is not the true one, as it only illustrates the load mobilized during the test. It is also clear that at the surface, $z = 0$, both curves show the same total pile bearing capacity, but at the pile toe, at $z = l$, where l is the pile length, the false load transfer curve shows a reduced point resistance value and an increased lateral resistance. The measured lateral resistance includes the true lateral resistance and the negative lateral resistance

#Corresponding author. E-mail address: brdanzig@uerj.br
[1]Universidade do Estado do Rio de Janeiro, Rio de Janeiro, RJ, Brasil.

Submitted on March 14, 2023; Final Acceptance on March 22, 2023; Discussion open until August 31, 2023.
https://doi.org/10.28927/SR.2023.002523

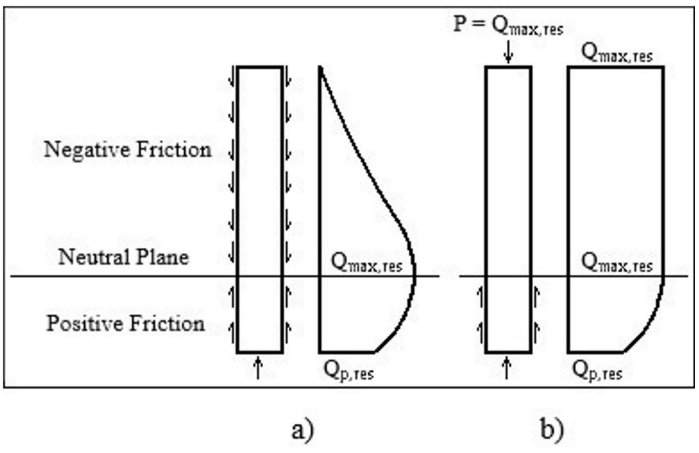

Figure 1. (a) Residual loads at pile shaft; (b) After loaded at the top with a load equal to the maximum residual load.

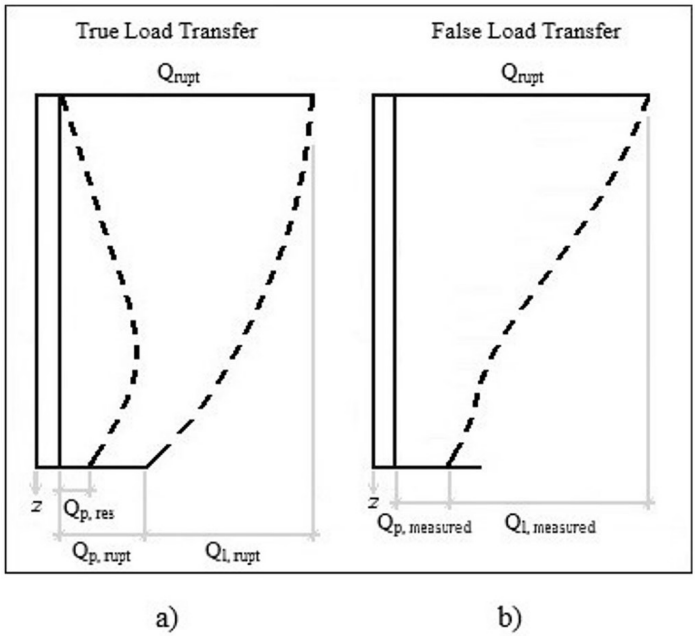

Figure 2. (a) True load transfer; (b) False load transfer.

locked into the pile shaft. The true lateral resistance is lower than the false while the true point resistance is higher than the false one, measured in a load test with instrumentation zeroed after driving or the previous loading.

According to Vesic (1977), the presence of residual loads results in an apparent concentration of skin resistance in the upper portion of the pile shaft which may cause a substantial reduction in the pile settlements. The cited author reported two projects he was involved in where the presence of residual loads had a relevant effect. In the first, the consideration of residual load resulted in a predicted settlement of one-sixth of what would be estimated by any conventional predictive method, with full confirmation by load tests. The second case consisted of the foundation of an eight-legged oil platform in the North Sea. Each leg rested on a group of four 1.80 m outside diameter steel pipe-piles. The previous settlement analyses considering varied assumptions of over consolidation ratio of the clay occurring in the soil profile showed a value of 25 mm at working loads, without consideration of residual loads. In a revised analysis, Vesic (1977) considered the presence of residual load and estimated a settlement of 10 mm, or even smaller. Vesic (1977) also warned about the doubtful value of several theories of pile settlement behavior published in the literature in recent years which do not consider the residual load phenomenon.

2. General historical review

This session addresses a brief report of the most relevant contributions to the issue. Some contributions are also included in more detail in the following sessions, as their data are revisited in the present paper.

Hunter & Davisson (1969) proposed an interpretation of load tests considering the effect of residual stresses due to driving. The authors clarified that the residual stress does not affect the ultimate tension and compression load capacity, but solely the magnitude of toe and friction load and their distribution along the pile.

A series of loading tests on precast instrumented concrete piles driven in loose sand was described by Gregersen et al. (1973). The loading tests indicated considerable axial forces in the pile after driving, with residual loads acting in opposite ways, downwards along the top and upwards along the pile bottom.

Residual loads were also registered by Cooke & Price (1973) in a long-instrumented friction pile jacked into clay. The friction pile remained in compression after the installation force had been removed.

Holloway et al. (1978) stated that unidimensional pile interpretation for driving and static load tests lead to a satisfactory simulation when compared to measurements of residual loads.

Cooke (1979) emphasizes that residual and friction forces at the shaft arise because of the different rates of mobilization of bearing forces at the base and friction forces at the shaft in the case of driven and jacked piles. In the case of bored, cast-in-situ concrete piles, Cooke (1979) found much smaller residual forces.

Briaud & Tucker (1984) observed that the most important factors influencing the distribution and magnitude of residual loads are ultimate point and total resistance, pile length and relative pile-soil stiffness.

Goble & Hery (1984) proposed a successive-blow analysis repeated until a convergence criterion is satisfied, following a procedure suggested by Holloway et al. (1978). This proposed analysis allows the estimate of permanent displacements and residual loads.

Poulos (1987) presented an analysis for estimating the initial stresses in a driven or jacket pile in three idealized profiles: soft clay, stiff clay and medium-dense sand. He concluded that the residual toe stress is a substantial proportion of the ultimate resistance for all three types of soil, but the values of residual toe stresses are most significant for piles in sand and least significant for piles in clay.

Darrag & Lovell (1989), based on analyses made with the program from Goble et al. (1988), presented charts and equations for estimating residual stresses after pile driving.

Randolph (1991) suggested an approach for implementing residual force analysis in the interpretation of stress-wave measurements. The author´s approach requires the application of the measured blow once or twice for each iteration of the soil parameters and avoids the need for multiple repetitions of the hammer blow.

Back-analyses of closed-ended pipe piles embedded in calcareous sand for an offshore platform were performed by Danziger et al. (1992, 1999). They found high residual stresses at the pile toe, most significantly for deeper penetration.

Massad (1992) describes a mathematical model based on observed pile behavior in cases where residual stresses are locked at the pile toe from the previous loading.

Rausche et al. (1996) presented an analysis including a sequence of several blows. They included three examples of the application and described the benefits and limitations of such an analysis.

Liyanapathirana et al. (1998) presented a FEM investigation of impact driving with soil modelled as an elastic perfectly plastic material simulating one single blow. This model was then extended by Liyanapathirana et al. (2000) to simulate multiple blows. The authors could visualize the residual stresses and the soil flows around the simulated piles.

Costa et al. (2001) presented a new interpretation of a wave equation program. Instead of following most dynamic analysis, as Smith's (1960), with the set determined indirectly by subtracting the quake from the maximum displacement at pile toe, Costa et al. (2001) proposition is distinct from this one. In this new program, called DINEXP, Costa (1988), the set is determined directly, as a final longer time is previously chosen, and pile toe displacement is calculated up to this time. This final time of analysis can be adjusted until a stabilized displacement at the pile toe is achieved. When residual stresses are locked into the pile toe the stabilized displacement is higher. The difference in set (stabilized displacement) determination is called by Costa et al. (2001) residual displacement. The residual stress in a pile final driving can thus be obtained. The load locked at the pile toe is equal to the soil toe stiffness (kN/m) multiplied by the residual displacement (m).

Fellenius (2002) illustrates in Figure 3 the CPT and SPT diagrams of a test site indicating a soil of uniform density and the loads measured at the strain gauge levels at plunging failure for the static loading tests in two piles of distinct lengths. The measured load distribution curves show, for both piles, a slight S shape curve, a steep to less steep and then steep again. The slope of the load transfer curve gives an indication of the mobilized shaft resistance in the soil. Fellenius (2002) observes that the slight S-shape suggests that the shaft resistance along the middle third of the pile is larger than along the lower third. The soil field tests do not support this observed behavior. Hence, it is concluded that the S-shaped curve is typical for the results of a test on a pile affected by residual load. In this case, the measured distributions do not show the true distribution of resistance of the pile. This fact is the basis of the author's procedure to determine the true resistance.

Zhang & Wang (2007) presented a large field instrumentation program for measuring residual forces in

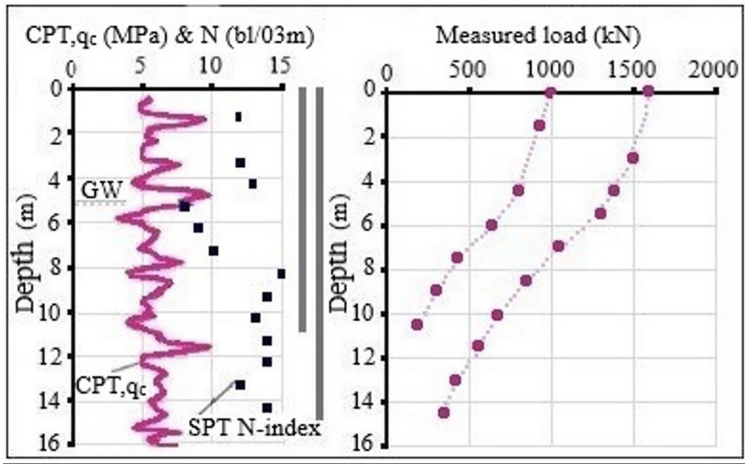

Figure 3. Field test results and measured load friction at the failure of two instrumented precast concrete piles, driven 11 m and 15 m into uniform loose sand, adapted from Fellenius (2002).

piles. The vibrating-wire strain gauges were installed before and after the installation was recorded. This study also verified that the residual forces increased when the test piles penetrated from weak layers into hard layers.

Kim et al. (2011) presented the results of a full-scale testing program involving two strain-gauge instrumented concrete piles, 600 mm outside diameter, at two nearby sites. The pile was driven to 56m, with its toe embedded into very dense sand. Three days after, the internal void was grouted. Kim et al. (2011) followed the build-up of residual load in the pile immediately after driving and up to 7 months later when static loading tests were carried out. The authors presented several results and emphasized that during the first 10 days, the strain changes were mostly due to temperature effects during hydration and swelling of the grout and concrete absorption of water from the ground.

Liu & Zhang (2012) presented the results of two 13 m long concrete pipe piles instrumented and then jacked. The field results showed that the post-jacking residual forces increased with the penetration depth. The maximum force that occurred at the neutral plane was found at 0.2 pile length above the pile toe.

Mascarucci et al. (2013) emphasized that even for cast in situ pile curing of the concrete can cause stress changes both in normal and shear stresses. In order to investigate the influence of residual loads on pile response to axial loading, they presented a parametrical study by numerical modelling.

Nie et al. (2014) compared the mechanism of residual stress in piles with negative friction after unloading. After instrumentation of a bored pile, they observed that residual stress distribution is similar to that occurring in presence of negative friction. In the case of residual stress, the adjacent soil mass prevents the pile from fully unloading.

Kou et al. (2016) instrumented five open-ended pipe piles with 13 or 18 m of embedded length. They found that the residual force increased when the pile penetrated the hard alluvium layer from the marine deposits. They also found that the residual force distribution along the test piles is highest at a position above the toe. The neutral plane is closer to the pile toe when the piles are embedded in a hard layer. Their conclusion is the same as reported by Costa et al. (2001) who observed that the higher the toe resistance, the closer the neutral plane is to the pile toe. For the same toe resistance, when the available shaft resistance increases with depth the neutral plane is deeper than when the available shaft resistance is quite uniform.

3. Measurement of residual loads

In this and the following two sections, a more detailed analysis is presented. Some most relevant research that includes residual loads measurements, load test interpretation considering the presence of residual loads and design procedures for estimating these loads are shown. The analysis is very useful to sections 6 and 7, broadening new possibilities and discussions of future development of the issue.

Gregersen et al. (1973) instrumented four precast concrete piles embedded into very loose sand on an island called Holmen, in the city of Drammen, Norway. Pile elements denoted as A, B and D were cylindrical, 280 mm in diameter and 8 m long. The pile element C was conical with a uniform taper varying from 280 mm, at the top section, to 200 mm at the toe.

Piles A and C were first tested separately as 8 m long piles. After completion of the tests on the 8 m long piles, they were connected to elements D and B, respectively, resulting in two 16 m long piles. They were denoted as pile D/A, with a cylindrical section, and B/C, cylindrical at the top and conical at the bottom section. The instrumentation was zeroed before driving. Figure 4a shows the results of piles A and D/A and Figure 4b of piles C and B/C.

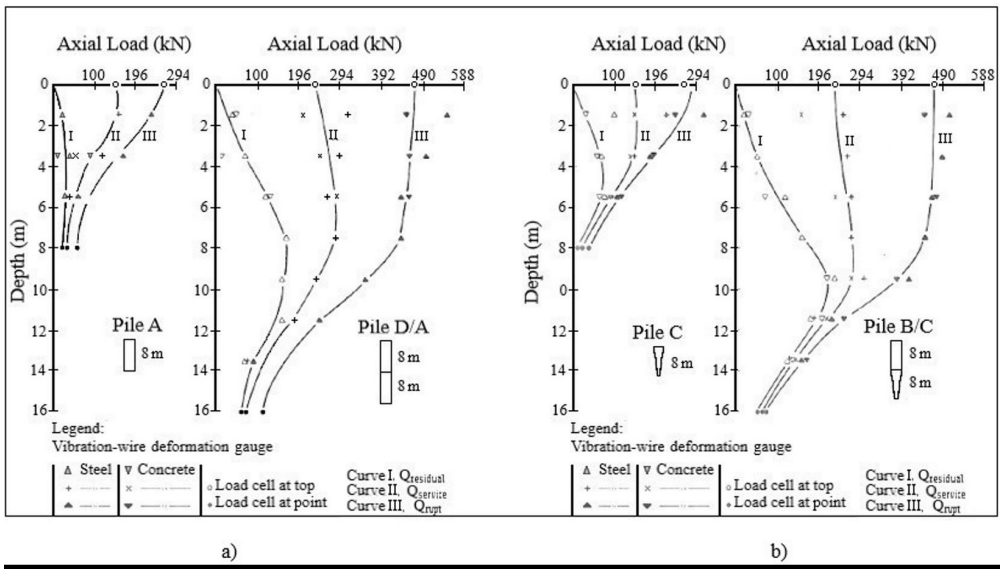

Figure 4. Compressive load on the pile with depth: (a) Piles A and D/A; (b) Piles C and B/C (adapted from Gregersen et al., 1973).

The authors verified considerable residual loads (type I curve) remaining in the piles after driving. The differences between the curves in the horizontal axis are related to the additional increment in external test loads applied to the pile top. The curves presented a similar pattern. The residual loads increase to a depth close to 2/3 the pile length, mobilizing negative skin friction, and then reduce from that level to the pile toe, mobilizing positive skin friction.

The hatched area in Figure 5 represents the false transfer curve for the service load of pile D/A. This is the curve that should be used for settlement estimation in design if the residual loads were known by measurement or prediction. This curve is obtained by the subtraction of the residual loads from the true transfer curve for service load measured when instrumentation is zeroed before driving.

Cooke (1979) instrumented a tubular steel pipe pile 0.17 m diameter and 5 m long, jacked into the London clay with undrained resistance of 35 kPa close to the surface and 78 kPa at 5 m depth. The limited travel of the hydraulic jack ram used in pile installation caused the need to unload the pile at each 0.10 m penetration. It was then possible to obtain the force-penetration diagram at 0.10 m intervals for the complete installation and the residual loads observed at each 0.1 m interval. Figure 6 presents the whole information, consisting of the continuous readings of the load cells in the pile shaft from the points where they passed beneath the ground level. At large penetrations, the residual loads at the pile base were approximately 75% of the maximum base load.

At several penetration levels, a pause was made for carrying out the incremental loading tests. The residual loads registered by the cells that had passed beneath the ground level were recorded and plotted in Figure 7. They were recorded in six different values of the penetration-diameter ratio. Cooke (1979) observed that at every ratio, the residual loads fall very close to the curve through all the load cell records obtained for full penetration of the pile. The author observed that this curve represented the unique residual load relationship, a clear indication of the shaft loading expected to occur for any length of pile less than the maximum penetration.

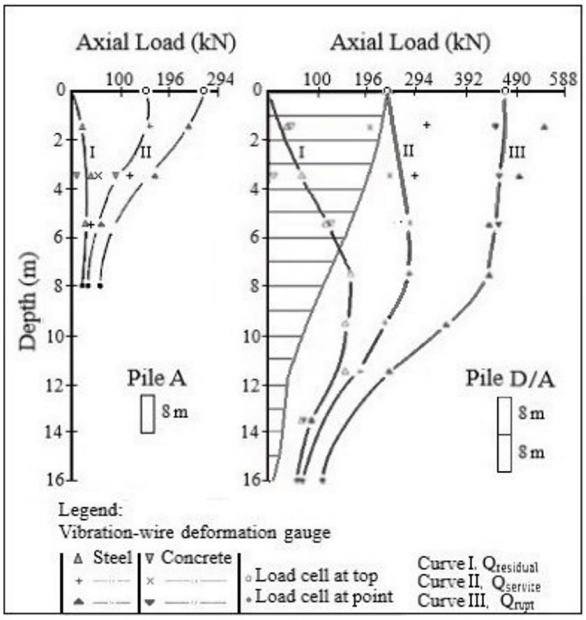

Figure 5. Hatched area illustrates the load transferred to the pile by the service load (adapted from Gregersen et al., 1973).

Rieke & Crowser (1987) presented an instrumented pile load test program for a bridge foundation in W14 x 145 steel-driven piles. The soil profile consisted of 15m of loose sand superposed to compact sand with gravel. The piles were 3 m embedded into the compact sand layer. The most

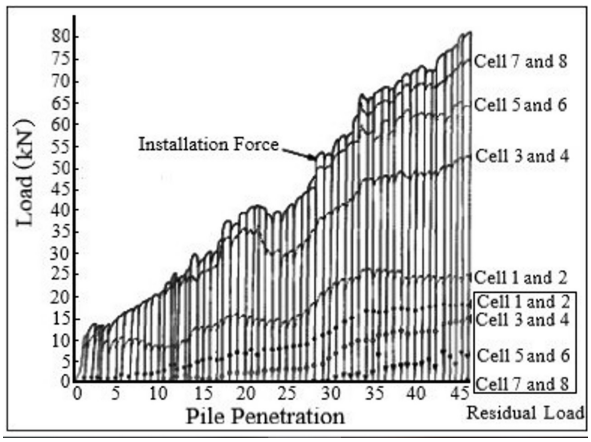

Figure 6. Installation force and pile loading at each cell position, illustrating the residual loads generated from each unloading of the pile (adapted from Cooke, 1979).

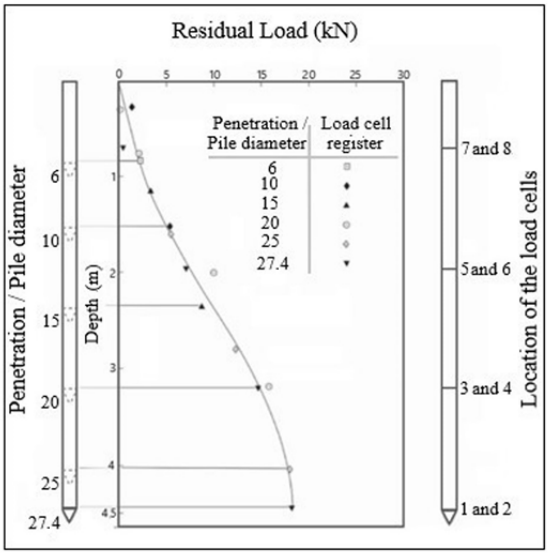

Figure 7. Residual load profile for all penetrations of the instrumented pile (adapted from Cooke, 1979).

relevant loading condition that controlled the project was the seismic loading that caused transient compressive and uplift loads. The authors observed relevant differences between the apparent (or false) and the true pile forces, a signal of the presence of residual loads. The soil was not susceptible to creep, but the authors observed that loading cycling can reduce, but not eliminate, the residual forces locked into the pile. Figure 8 illustrates the residual forces observed after driving, before the tension test, and obtained after the tension test. Rieke & Crowser (1987) concluded that both tension and compression load cycles can modify soil stresses from the original post-driving residual condition and that

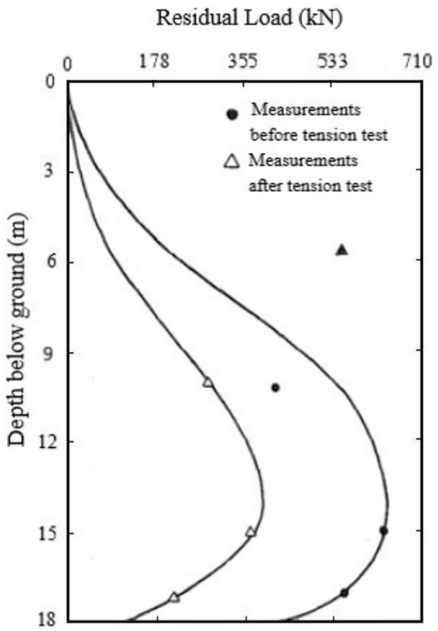

Figure 8. Residual forces in the pile before and after the tension test (adapted from Rieke & Crowser, 1987).

the reduction in residual forces continues with additional cycles, but it is not eliminated. The authors identified two factors that can produce changes in residual loads in piles: the loading history in the case of cyclic loadings and the soil creep that can cause stress relaxation with time in plastic soils susceptive to secondary consolidation.

Briaud et al. (1989) presented an instrumented loading test of a pile group in a sandy profile and a single pile instrumented as a reference. The geometry of the closed-end-driven pile, the embedded length and the soil profile are shown in Figure 9. The instrumentation was part of a research project in San Francisco, California. The results consisted of the residual load distribution in the piles after driving, the load settlement curve of the single pile and the pile group, the load transfer curves and the maximum friction versus depth profile. Figure 10 shows the comparison between the load versus depth for different loading increments for the single pile and the central pile in the group.

The single pile presented a residual point load of 61 kN which is 11% of the ultimate point resistance. Piles in the group presented a residual load of 10 kN. Briaud et al. (1989) attributed this behavior to the fact that close to full penetration the pile driving loosens the prestressing existing under the toe of neighbouring piles.

The capacity of the group was 2499 kN, while the capacity of the single pile was 505 kN, an efficiency of 99%. At failure, the friction load of the single pile was 147 kN while the average friction load of the average pile in the group was 269 kN, a friction efficiency of 183%. The efficiency of the

point was 67%. Briaud et al. (1989) observed that a group of end-bearing piles may have efficiencies lower than 1, while a group of friction piles may have efficiencies higher than 1.

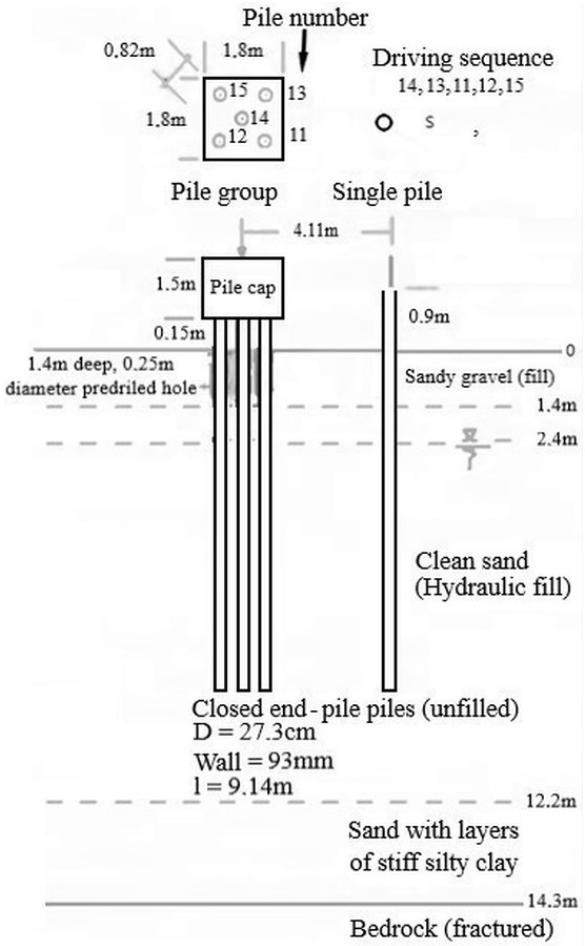

Figure 9. General test conditions (adapted from Briaud et al., 1989).

4. Load test interpretation for obtaining the residual loads

Decourt (1989) noted residual loads in piles caused by the previous loading. The significant change in the load transfer caused by the residual loads resulted in the author´s suggestion of increasing the service load of excavated piles.

In a bidirectional static load test, an expansive cell is concreted together with the pile. The hydraulic activation of the cell causes its expansion, pushing the shaft upwards and the toe downward. The upward and downward displacements can be measured at cell levels (bottom and top) and the pile top. The reaction system is provided by the pile shaft and the test is carried out up to the exhaustion of the tip or friction capacity. At this moment:

$$Q_{p,mobilized} = Q_{l,rupt} \tag{1}$$

and:

$$Q_{t,\ mobilized} = Q_{p,mobilized} + Q_{l,rupt} = 2Q_{l,rupt} \tag{2}$$

Where $Q_{p,mobilized}$ is the toe resistance mobilized in the test that is in equilibrium with the available lateral resistance, considering the simplified premise that negative and positive skin frictions are equal. $Q_{l,rupt}$ is the ultimate lateral resistance, exhausted during the load test, and $Q_{t,mobilized}$ is the total capacity mobilized in the test.

Decourt (1989) suggests that the expansive cell should be grouted and attached to the pile. The service load could then be increased to a value up to the lateral friction mobilized in the second loading (false curve), which value would be at least double the lateral friction mobilized in the first loading. According to Figure 1, up to a load of $Q_{l,rupt}$ practically no loading would be added to the pile shaft below the neutral plane, and the lateral friction above the neutral plane would be zeroed. If the load at the pile top is raised to

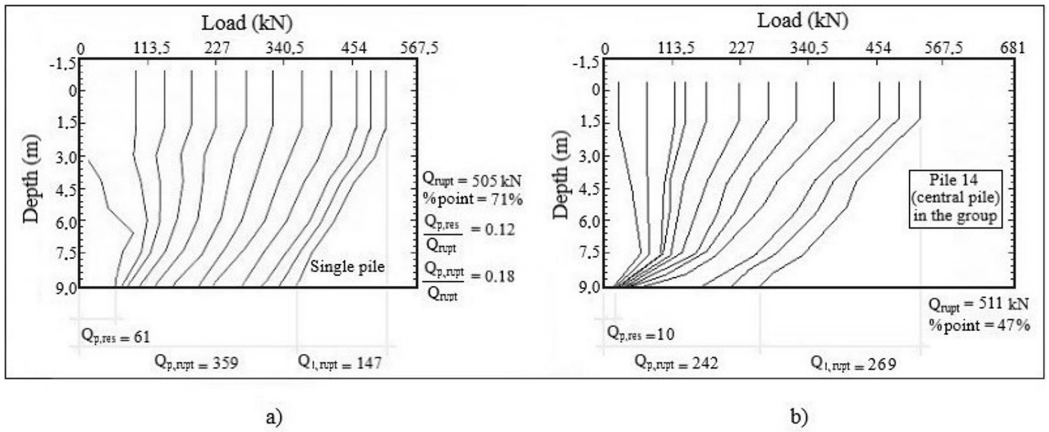

Figure 10. Load versus depth for (adapted from Briaud et al., 1989): (a) Single pile; (b) Pile 14, central pile in the group.

$2Q_{l,rupt}$, the added load would be mobilized by the positive friction above the neutral plane and the increase in the toe load would be negligible. In this condition, the settlement would be very small.

The author of the present article emphasizes two relevant issues not considered by Decourt (1989): i) although Decourt (1989) considers that friction resistance is the same in compression and in tension, which is on the safe side, the global safety factor of two is not assured if the service load is equal to $2Q_{l,rupt}$. The global safety factor of 2 is only assured if Q_{rupt}, the sum of $Q_{p,rupt}$ plus $Q_{l,rupt}$, is higher than twice the service load. ii) another simplification that is not emphasized by Decourt (1989) is the consideration of $Q_{p,residual}$ equal to $Q_{max,residual}$; it is true only if the neutral plane is at the pile toe, occurring only if the toe resistance is much greater than the lateral resistance. It is not the general case, as indicated by the piles instrumented by Gregersen et al. (1973) and Cooke (1979); iii) the cyclic loadings and the soil creep, which can cause stress relaxation over time in plastic soils susceptive to viscosity effects, must be considered in the design.

After the experience of interpreting nine (9) static load tests, most of them in instrumented piles, Decourt (1991) developed a simple method that can separate the toe and lateral resistance for piles not instrumented during the static loading test. The rebound method, as named by Decourt (1991), has the premise that the lateral resistance is the same, at compression and tension loading. As shown in Figure 2, after driving a displacement pile or after the first loading of a non-displacement pile, the true lateral load, $Q_{l,rupt}\ (T)$, can be obtained by Equation 3. In Equation 3 $Q_{l,\,measured}\ (F)$ is the apparent, or false, lateral load, measured during a second loading of the test, and $Q_{p,\,residual}$ is the unknown residual load locked into the pile toe after the previous loading. From Equation 3, Equation 4 can be easily written.

$$Q_{l,rupt}\left(T\right) = Q_{l,measured}\left(\mathrm{F}\right) - Q_{p,\,residual} \tag{3}$$

$$Q_{p,residual} \leq Q_{l,rupt}\left(T\right) \tag{4}$$

The second loading in a loading test, according to Decourt (1991), has to be carried out up to at least twice the true lateral resistance, $Q_{l,rupt}$, according to Equation 5.

$$Q_{t,2} \geq 2Q_{l,\,rupt}\left(T\right) \tag{5}$$

In order to obtain $Q_{l,rupt}\ (T)$, Decourt (1991) suggests considering the loading corresponding to the displacement of 10 or 15 mm in the first loading curve, or half of the loading corresponding to the pile rebound ($Q_{rebound}$).

In order to determine $Q_{rebound}$, Decourt (1991) proposed the graphical solution illustrated by Figure 11.

The pile rebound, δ_{re}, in Figure 11 is the recoverable settlement of the second curve, known as the elastic settlement, which corresponds to the Q_{re} in Figure 11. This rebound settlement, δ_{re}, is due to load transfer from the false $Q_{l,measured}$ in Equation 3. From Equations 3 and 4 it can be concluded that Q_{re} is at most equal to twice the $Q_{p,residual}$ and $Q_{l,rupt}$ or, inversely, $Q_{p,residual}$ or $Q_{l,\,rupt}$ is at least equal to half of Q_{re}. Table 1 indicates that half of Q_{re} is a satisfactory approximate prediction of the lateral resistance estimated as Q_{10}, Q_{15}, or Q_{DQ}, the last being the estimated value by Decourt & Quaresma (1978). The half of Q_{re} is also a prediction of the residual load locked into the pile after a prior loading.

Continuing with the interpretation of load tests in the presence of residual loads, Massad (1992) presented a general mathematical model for both displacement and non-displacement piles that can separate the lateral and the toe resistance from the total capacity, including the residual load locked at the pile toe for homogeneous soil. Massad (1993) extended the model in the case of piles with an embedment into a much more resistant layer.

The presence of a residual load occurring at the pile toe explains the higher stiffness of the load x settlement curve in the second loading compared to the initial loading, as shown in Figure 12. Point A of the curve, in the first loading, is shifted

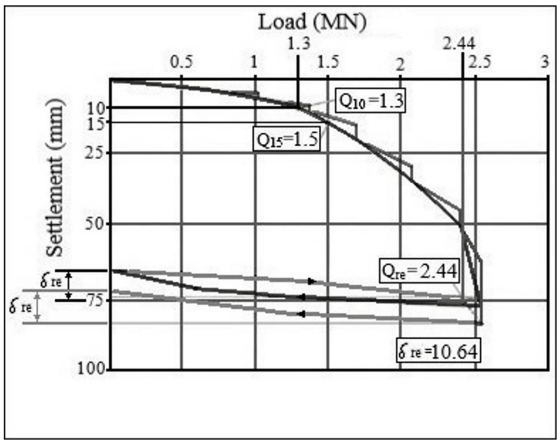

Figure 11. The Rebound Method, adapted from Decourt (1991).

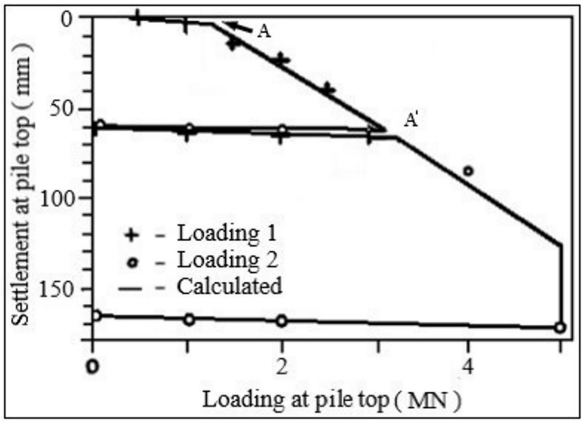

Figure 12. Load versus settlement curve at top of an excavated pile at USP Research Field (adapted from Massad, 1992).

Table 1. Different suggestions for $Q_{l,rupt}$ (adapted from Decourt, 1991).

Test	Q_{10}	Q_{15}	Q_{DQ}	$Q_{re}/2$
1	1.30	1.50	1.08	1.22
2	0.95	1.18	1.16	1.20
3	1.62	1.85	_	>1.25
4	2.60	3.44	2.28	2.33
5	2.37	3.05	3.47	2.87
6	2.98	3.20	_	3.34
7	1.31	1.55	1.99	1.59
8	0.48	0.54	0.54	>0.29
9	2.15	2.40	_	>1.65

to the right, A´, in the second loading curve, characterizing the presence of residual load in the pile. The stiffness in the unloading phase is recoverable in the second loading and its large elastic extent is caused by the residual loads. The estimated curve obtained by Massad (1992) model in Figure 12 matched the experimental results very closely.

Massad (1992) defined the coefficient μ, in Equation 6, which considers the effect of the residual load in the model.

$$\mu = 1 + Q_{p,res} / Q_{l,rupt} \quad (6)$$

Massad (1992) modified the Camberfort Laws to consider the presence of residual loads and the reversion in lateral friction. He also showed that in a more general aspect, the load versus settlement curve in a static pile test consists of four (4) loading and three (3) unloading ranges. Massad (1992) used the proposed method to analyze each loading and unloading range and presented the formulations that allow the estimation of the model parameters in numerous cases, including rigid and flexible piles embedded into uniform soil layers or embedded partly in a residual soil or rock, Massad (1992, 1993, 1995, 2001), Massad & Lazo (1998), Fonseca et al. (2007), Marques & Massad (2004), Mussara & Massad (2015), among other contributions.

Fellenius (2002) proposed a simple graphical method to obtain the true load and residual load transfer from the measured (false) transfer curve in an instrumented load test, illustrated in Figure 13 in a case of homogenous soil. Fellenius (2023) also applies the method to the results from dynamic load tests. The method assumes that the shaft resistance measured along the upper length of the pile is the false resistance. The true resistance is considered equal to the negative resistance, and both are equal to half of the measured resistance. That is, the false distribution incorporates negative shaft friction and positive true friction. Fellenius (2002) begins the true curve by tracing half of the false curve. The other half corresponding to the negative friction is considered the residual load. Below the 8 m depth in Figure 13 the increasing rate of the transfer curve is reduced because of the proximity of the neutral plane. The true curve is the sum of the residual and the measured curve. For a homogeneous soil profile, Fellenius (2002) proposes the extrapolation of the true curve by adjusting the beta value of the positive friction on the superior branch, Equation 7.

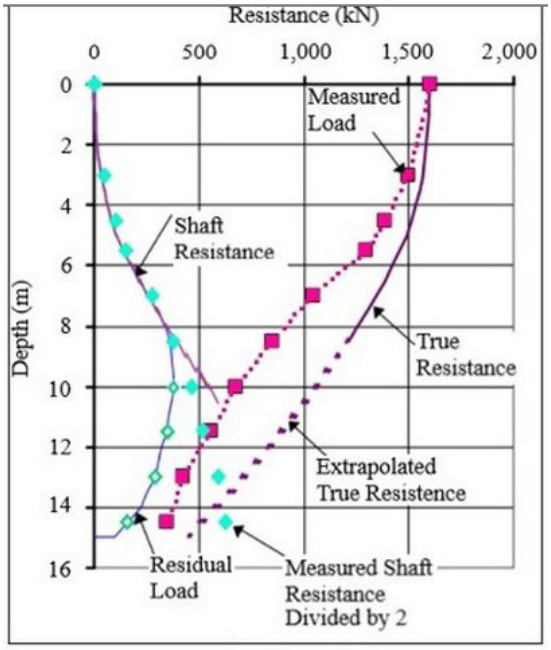

Figure 13. The graphical method (adapted from Fellenius, 2002).

$$\tau_{rup} = \beta \sigma_v' \quad (7)$$

Finally, Fellenius (2002) completes the residual load distribution below the neutral plane by subtracting the measured curve from the true load.

Fellenius (2002) emphasizes that in inhomogeneous soil, with water pressure different from hydrostatical, adjacent piles or nearby excavations, it is necessary to use special software. Fellenius (2002) also point out that the method should also be applied with a good soil characterization.

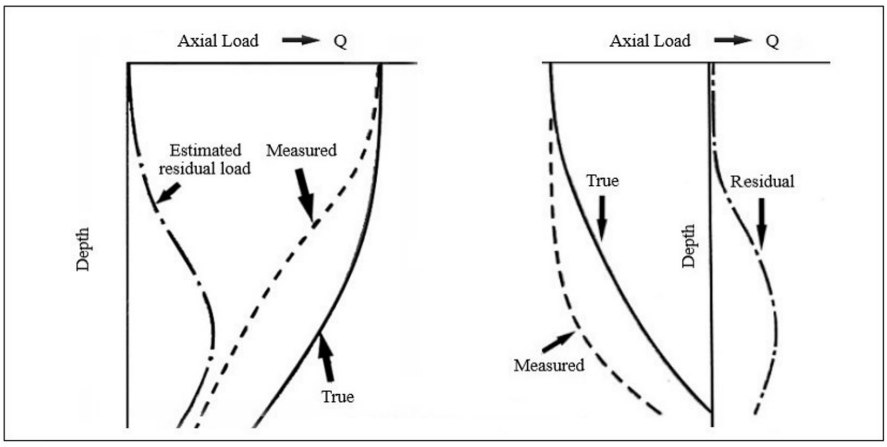

Figure 14. Comparison between the static and tension load tests (adapted from Holloway et al., 1978).

5. Methods for estimation of residual loads

Holloway et al. (1978) proposed a wave equation solution in finite differences, as proposed by Smith (1960), coupled with a static equilibrium solution after attenuation of the energy imposed on the pile from driving. This solution originated the RSA (Residual Stress Analyses) version of the GRLWEAP program (wave equation analysis). Holloway et al. (1978) showed a scheme of the load transfer of an instrumented static load pile in compression and another in tension, with the instruments zeroed before the load test, and not before the driving installation, Figure 14a and b. The residual stresses were estimated by the authors. Although in the static compression load test the true distribution is higher than the measured one, in the tension test the opposite occurs.

Briaud & Tucker (1984) proposed a prediction method to obtain the residual loads in piles embedded into sands. Even recognizing the proposition as a simple method having many simplifying hypotheses, the main advantage of the method is the ability to observe the factors influencing the residual loads.

Briaud & Tucker (1984) started with a failure condition, shown in Figure 15, and established the equilibrium equation to an elementary pile section, resulting in a differential equation. Applying the boundary conditions, they arrived at Equation 8, expressing the residual loads with depth.

$$Q_{z,\,res} = Q, z_u \; - \; Q_{rupt} \left[\begin{array}{c} (E_p \;\omega + \; K_p^{'})\, e^{\omega(L-z)} - \\ \dfrac{(E_p \;\omega - \; K_p^{'})\, e^{-\omega(L-z)}}{(E_p \;\omega + \; K_p^{'})\, e^{\omega L} - } \\ (E_p \;\omega - \; K_p^{'})\, e^{-\omega L} \end{array} \right] \quad (8)$$

$$\omega = \sqrt{K_\tau^{'} P \Big/ E_p}$$

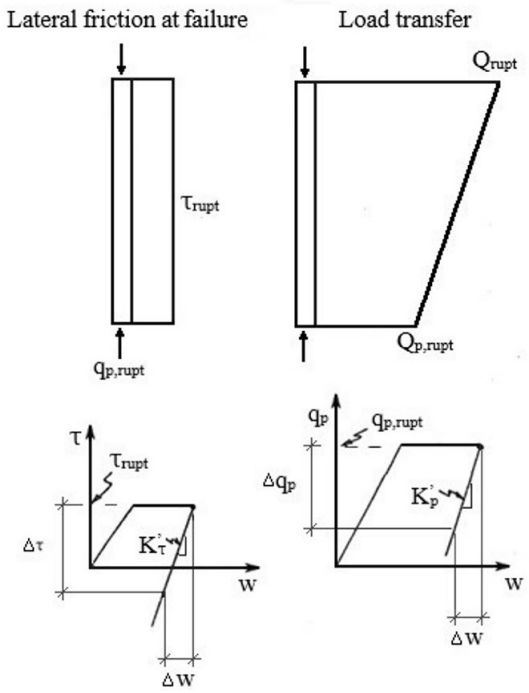

Figure 15. Unloading process starting from failure (adapted from Briaud & Tucker, 1984).

$Q_{z,residual}$ is the residual load at depth z
P is the pile perimeter
$E_{p,}$ is the pile Young modulus
$K_\tau^{'}$ and $K_p^{'}$ are shown in Figure 12.

The residual load at a pile toe can be obtained by setting $z = L$, in Equation 8, resulting in Equation 9.

$$Q_{p,res} = Q_{p,rupt} - \left[\frac{2Q_{rupt}}{\left(1+\dfrac{E_p\,\omega}{K_p^{'}}\right)e^{\omega L} - \left(1-\dfrac{E_p\,\omega}{K_p^{'}}\right)e^{-\omega L}} \right] \quad (9)$$

The authors concluded that the distribution of residual loads depend on the failure load at pile point, the total failure load, the pile length and the pile and soil relative stiffness.

Although considering the dynamic analysis as the most adequate, Poulos (1987) presented a simple static method of residual loads estimates for driven and jacked piles. In this simplified estimate of residual loads, Poulos (1987) applied a static analysis for the final penetration in which the pile is loaded to failure and then unloaded. The analysis is the same as that of Poulos & Davis (1980), enabling the pile and soil relative displacement and incremental loading and unloading. The analysis was implemented in a software that includes the installation, static loading and unloading.

The same 50 m long pile with 1 m diameter was considered, with three different types of Young's modulus: stiff (E_p = 250 GPa); a moderate (E_p = 25 GPa) and extremely compressive pile (E_p = 2.5 GPa). Poulos (1987) pointed out that only the second case is of practical relevance, corresponding to a concrete pile. Table 2 summarizes the cases included in Poulos (1987)´s studies.

For the intermediate pile stiffness (E_p = 25GPa), Figure 16 shows the estimated residual shear stresses along the pile shaft for the three soil types. The limiting shaft resistance values for both compression and tension loading are also shown. The residual shear stress is either negative or positive, above and below the neutral plane, respectively. In the sandy profile, and because of the high point resistance, the residual shear stress may be negative throughout the pile.

Figure 17 shows the estimated distributions of the pile shaft residual load for the three pile stiffness values. It shows that the stiffer the pile, the smaller the pile shaft residual loads. In sandy soils, the neutral plane approaches the pile toe.

Darrag & Lovell (1989) reported that the wave equation analysis is the only analytical procedure that includes all important factors contributing to residual stresses. Darrag & Lovell (1989) utilized the earlier CUWEAP wave equation program, developed by Hery (1983) to develop a simplified procedure for predicting residual stress range and distributions. The authors ran the CUWEAP program more than 250 times to produce a set of charts to predict the residual stress percent (a_r) for a sand profile normally consolidated in its original condition. The charts include concrete and steel piles, and a typical chart is illustrated in Figure 18.

In Figure 18, a_r provides the ratio of residual load at pile toe to pile point capacity, in percentages. The authors produced the charts for m= 40%, m being the ratio of shaft resistance to total pile resistance, in percentages. For m values other than 40%, Equations 10, 11, 12 can be used to obtain a corrected value for a_r.

$$(a_r)_{m\%} = (a_r)_{m=40\%}\, x\beta \tag{10}$$

$$m < 55\ \% \beta = 0.025\ x\ m \tag{11}$$

Table 2. Cases analyzed by Poulos (1987).

Case	Soil profile	Soil Modulus		$f_{s,\,rupt}$	
		E_0 (MPa)	N_v (MPa/m)	$f_{s,z=0,rupt}$ (kPa)	β (kPa/m)
A	Stiff clay	50	0	75	0
B	Soft clay	0	1.0	0	1.5
C	Sand	0	1.5	0	2.0

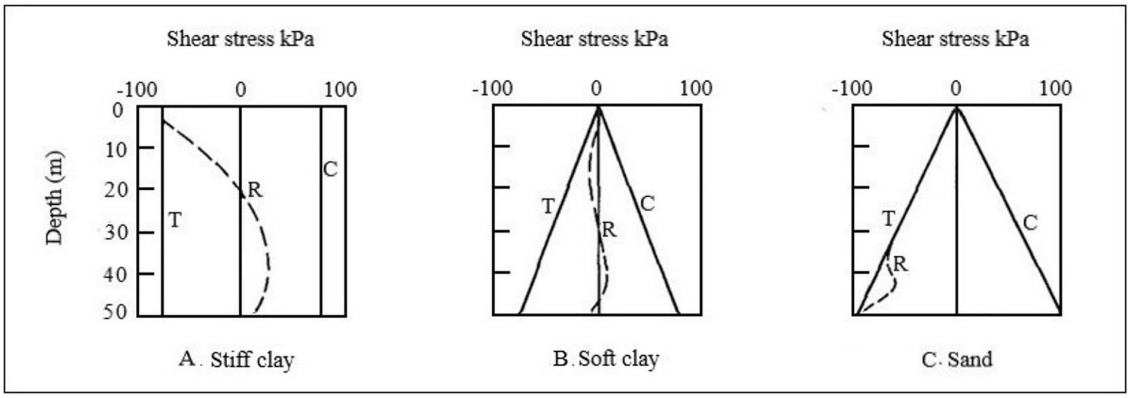

Figure 16. Residual stresses estimated for the three soil types, E_p = 25 GPa. *R*, residual stresses; *T*, failure stresses in tension; *C*, failure stresses in compression (adapted from Poulos, 1987).

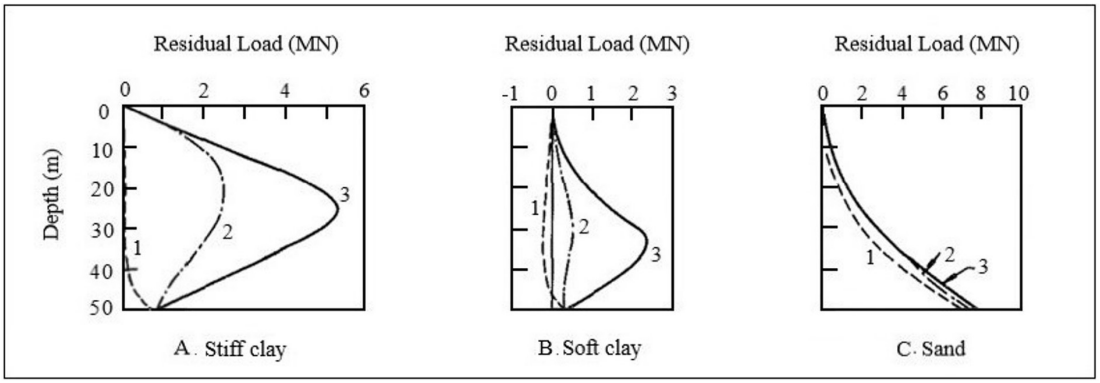

Figure 17. Distribution of residual load: Curve 1, E_p = 250 GPa; Curve 2, E_p = 25 GPa; Curve 3, E_p = 2.5 GPa (adapted from Poulos, 1987).

$$m > 55\ \%\ \beta = 1.375 + 0.01\ (m - 55) \qquad (12)$$

Costa et al. (2001) presented a new finite element solution developed by Costa (1988) to analyze the pile during driving. One important feature of the DINEXP program is the possibility to estimate the residual stress. Instead of estimating the set as most pile drivability programs do, the maximum displacement minus the quake, DINEXP calculates it directly as the stabilized displacement occurring when toe particle velocity approaches zero. It is noticeable that the stabilized displacement is higher than the set calculated in most solutions. The difference is attributed to the residual load locked in the pile during unloading and causing an incomplete rebound. Figure 19 illustrates the difference.

If the elastic residual displacement, *a* in Figure 19, is multiplied by the soil stiffness at the pile toe (toe capacity divided by toe quake) the pile toe residual load is obtained. Figure 20 presents a typical comparison of the set *s* calculated by most drivability programs and that determined directly.

Costa et al. (2001) proposed the application of this new procedure to estimate the permanent pile displacement and the residual loads locked in the pile at the end of driving. The authors confirmed an existing conclusion established by the main research in the literature and disclosed some new aspects. The residual toe load ratio to total bearing capacity first increases and then decreases with the increase of the toe to total resistance percentage. With the increase in toe resistance percentage the neutral plane deepens, approaching the pile toe. Considering the shaft friction distribution, the higher the toe resistance percentage the lower its influence on residual loads.

6. Comparison of different residual load estimation proposals to main instrumented solutions

An initial comparison will be shown for a typical hypothetical steel pile double I section (12 x 4 5/8 inches), 154.6 x 10^{-4} m^2 cross section, 20 m long, E_p = 210 GPa driven into a sand deposit of varying density. For a total capacity of 2400 kN and toe percentage varying from 20%, 50% and 80%, the solutions from Briaud & Tucker (1984), Darrag & Lovell (1989), GRLWEAP (Goble et al., 1988), Costa et al. (2001) are compared in Figure 21. Because Briaud &Tucker (1984) considered a constant unitary friction along the pile shaft, the same premise was considered in Figure 21 for the other methods, except for the Darrag & Lovell (1989) charts which were based on unitary friction increasing linearly with depth.

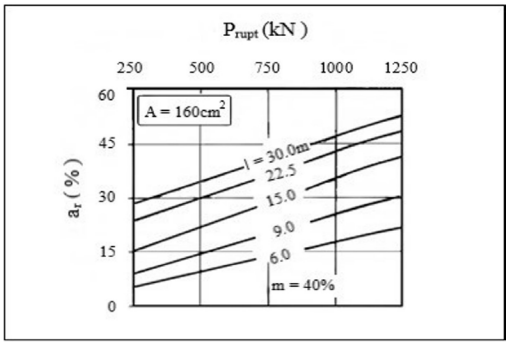

Figure 18. Typical Darrag and Lovell chart for steel pile with cross section *A* and length varying from 6 to 30m (adapted from Darrag & Lovell, 1989).

Most solutions first show an increase and then a decrease of the residual toe load ratio to total capacity versus the point to total capacity. Only the GRLWEAP in its 2001 version showed a residual load ratio to total capacity always increasing with the toe resistance percentage, a feature differing from the other solutions, even for a previous version of the same program, CUWEAP. The Darrag & Lovell (1989) charts indicated the maximum residual toe load to total capacity at the same toe percentage as the Costa et al. (2001) solution. Although the Briaud & Tucker (1984) equations were based on many simplified assumptions, their results are close to more complete solutions, except the toe percentage related to the maximum residual load.

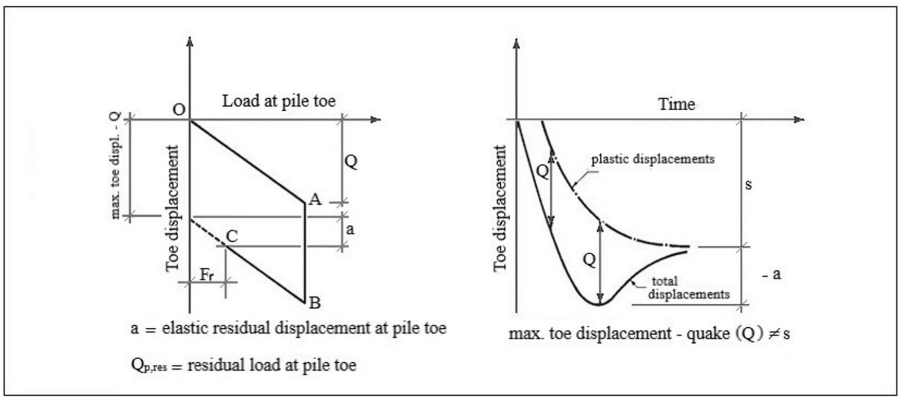

Figure 19. Load versus displacement and displacement versus time when residual loads occur at pile toe (adapted from Costa et al., 2001).

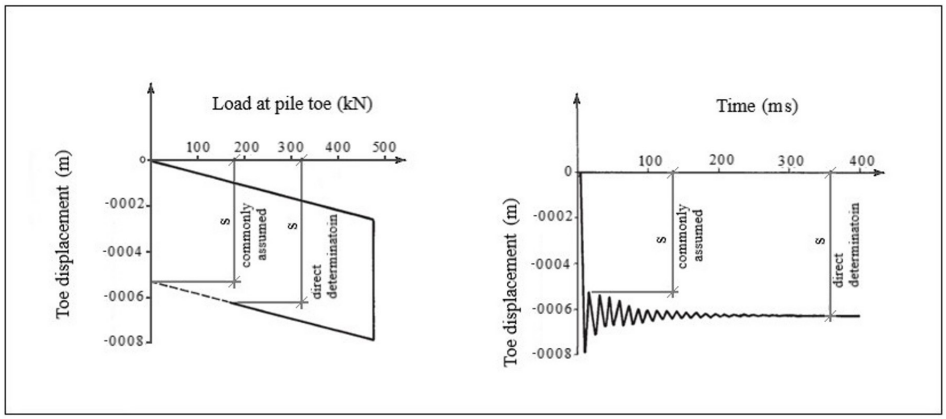

Figure 20. Different features of set determination (adapted from Costa et al., 2001).

For the Costa et al. (2001) solution, a comparison was made for two distinct unitary friction variation: a uniform, the same shown in Figure 21, and a linear variation. For the linear variation, the GRLWEAP solution is also shown in Figure 22.

Figure 22 shows two types of curves. The upper curves express the residual toe load ratio to point resistance, here named toe mobilization ratio, and the lower curves express the residual toe load ratio to total capacity. For the low point resistance percentage, both curves differ widely, but for a higher point resistance percentage they come closer to each other as the point resistance percentage approaches 100%. In fact, for low point resistance percentage, the shaft friction is high, thereby the friction distribution plays a different role, mainly in the toe mobilization ratio. For high point resistance percentage, the curves tend to intercept. The yellow region diminishes its area as point resistance percentage approaches 100%.

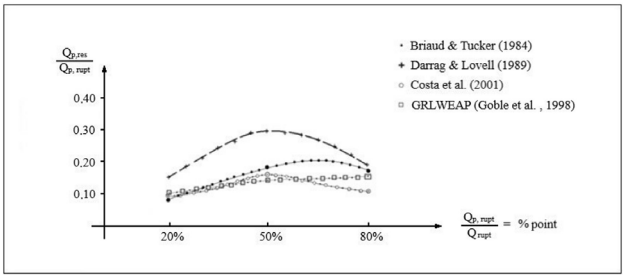

Figure 21. Residual toe load ratio to total capacity versus percentage of point to total resistance for different solution.

7. Comparison of residual load estimation proposal to main instrumented solutions

Zhang & Wang (2007) described an extensive instrumented field-monitoring program for studying the residual loads in long steel driven piles. Eleven H piles were instrumented, monitored and load tested. They have a 285 x 10^{-4}m^2 section and length varying from 34.2 m to 59.8 m. The soil profile consisted of a fill layer, marine deposits, an alluvium layer and fully or moderately decomposed granite. The piles were driven and embedded into the decomposed granite. Danziger & Lopes (2008) interpreted the whole database and selected the same dimensional values, the measured point resistance percentage at failure obtained in the static instrumented test in the horizontal axis and the residual toe load ratio to total capacity in the vertical. Figure 23 shows that the instrumentation

follows the same pattern of the prediction curve in Figure 22. Only one of six instrumented piles with complete data, named IB3-3, fell outside a line passing through the instrumented piles.

Ganju at al. (2020) presented the results of a static and two (2) dynamic load tests performed on a closed-ended steel pile of 0.6 m outside diameter and 18m long. Locked-in residual loads were measured at the end of driving and used to correct the pile capacity components measured at the static load test. The soil profile consisted of several layers of sand and gravel mixtures.

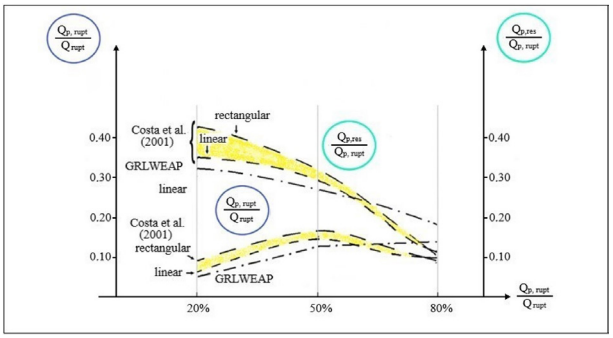

Figure 22. Influence of variation in unitary friction: uniform (rectangular) and linear.

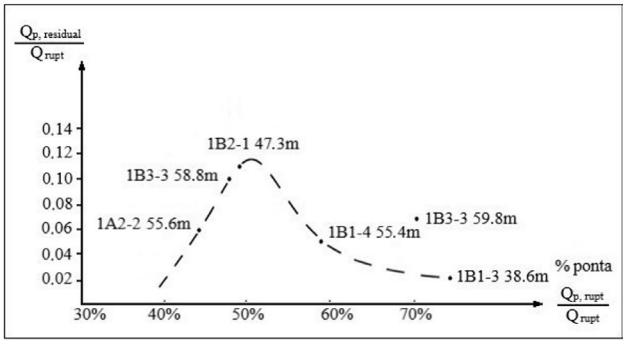

Figure 23. Zhang & Wang (2007) (data interpreted by Danziger & Lopes, 2008).

Figure 24 shows, on the left, the blow counts per unit length of pile versus depth and on the right the SPT blow counts, soil profile, and CPT q_c results. Driving resistance peaked at 7.5 m penetration, on the same horizon where the soil profile indicated a gravelly sand and the N_{60} and q_c profile registered a sharp increase.

Figure 25 illustrated the measured residual loads at the end of driving and the unitary friction. Figure 25 follows the same pattern observed in Figure 4 by Gregersen et al. (1973) in concrete piles in a sandy profile.

Figure 25 illustrates, at 7 m depth on the right, the corrected true unit shaft resistance of 58 kPa as the sum of the false shaft resistance, 98 kPa, and the -40 kPa negative unit shaft friction. The maximum negative unit shaft resistance is 70% of the true shaft resistance at 7 m depth.

Figure 26 is obtained if the whole instrumented database in sandy soils is now superposed in the same dimensionless axis as the curves representing Costa et al. (2001) analysis.

The calculated pile stiffness is included in the table within Figure 26. The first four (4) piles in the table are the precast piles from Gregersen et al. (1973). The 8m pile with uniform section has the same stiffness as the steel piles of Costa et al. (2001). Its position coincides with that of the curve for linear unitary shaft friction distribution of Costa et al. (2001), not only for the mobilization ratio curve but also for the toe residual load ratio to total capacity. The conical pile with a uniform taper is less rigid than the uniform section pile. Because of its small section at pile toe, it has a smaller percentage of point resistance and is positioned on the left in the horizontal axis in Figure 26, in a region not covered by Costa et al. (2001) analyses. However, its position is within the possible extrapolation of the mobilization curve and the curve expressing the toe residual

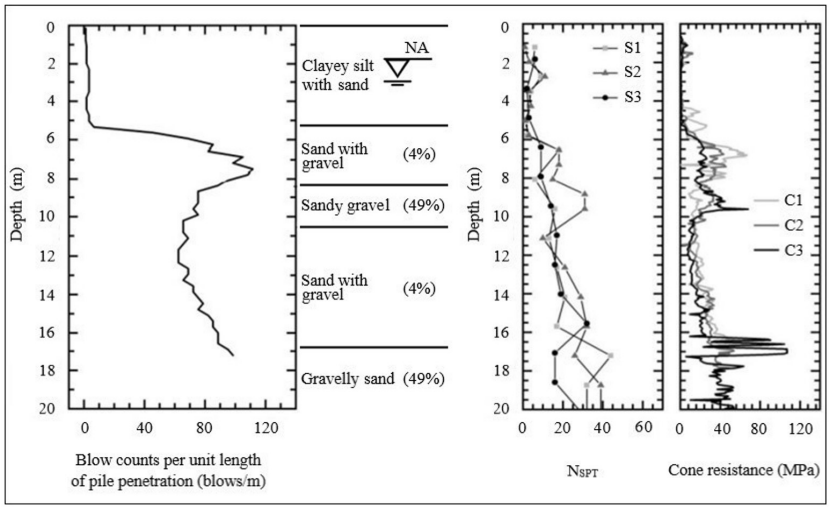

Figure 24. Blow counts during pile penetration compared do field tests (adapted from Ganju et al., 2020).

load ratio to total capacity. The corresponding 16m long piles from Gregersen et al. (1973) are more flexible piles, and both are positioned in Figure 26 above the 8m piles. It agrees with the Poulos (1987) findings that the stiffer the pile, the smaller the residual loads. Another aspect that is clear in the position of the data from Gregersen et al. (1973) is its parallelism to the Costa et al. (2001) curves. While the 8 m piles are positioned very close to the Costa et al. (2001) curves, the more flexible 16 m piles indicate higher residual loads but with the same variation with the point percentage.

The following instrumented pile in Figure 26 is the single pile from Briaud et al. (1989). Its stiffness is very close to the pile studied by Costa et al. (2001). While Gregersen et al. (1973) precast concrete piles were embedded into a very loose sand, the single steel pile instrumented by Briaud et al. (1989) is embedded into a much denser sand with a high point resistance percentage, positioned to the right of the horizontal axis. This Briaud et al. (1989) pile is also positioned very close to Costa et al. (2001) curves, as illustrated in Figure 26.

The next pile on the list is that instrumented by Ganju et al. (2020). Although its stiffness is one and a half times higher than the reference pile from Costa et al. (2001), its position is also very close to the curves from Costa et al. (2001). The last pile driven in sand analyzed herein is from Rieke & Crowser (1987), the stiffness of which is more than twice the reference pile used by Costa et al. (2001) to construct their curves. In fact, it is

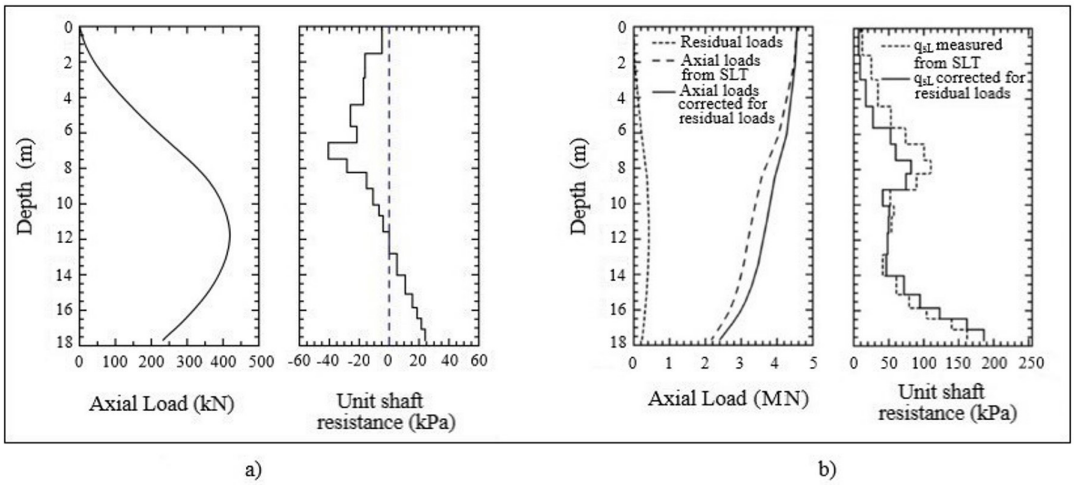

Figure 25. (a) Residual axial loads and unit shaft friction; (b) measured and corrected load transfer curves and unit shaft resistance at failure (adapted from Ganju et al., 2020).

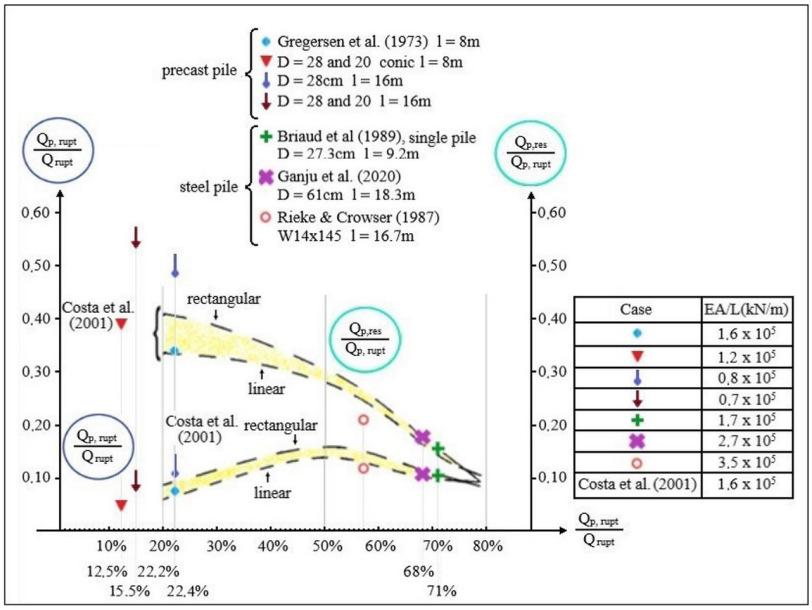

Figure 26. Documented cases including measured residual load in concrete and steel piles in sandy soil.

positioned below the Costa et al. (2001) curves, in agreement with Poulos (1987), Briaud & Tucker (1984) and others.

Revisiting the results from Cooke (1979), who measured the total, the point and, by difference, the lateral friction of a single pile continuously, in addition to the residual load, it was possible to interpret the same data positioning them in the same dimensionless axis of the previous documented cases in sand. A series of piles of varying length were now considered for the same penetration interval used in Cooke (1979) experiments. The longer the piles, the lower their point resistance in a uniform soil layer. Cooke (1979)'s tubular steel pipe pile, 0.17 m diameter, jacked into London clay was then interpreted as a series of piles with varying L/D ratios. The series of data was expressed in the same two curves obtained by Costa et al. (2001). All data were gathered in Figure 27.

Although presenting few outliers, the main data in Figure 27 have very clear behavior. The lower curve shows the same pattern first observed by Danziger & Lopes (2008) who pointed out that: if the measured point resistance percentage at failure is fixed in the horizontal axis and the toe residual load ratio to total capacity is positioned in the vertical axis, the resulting curve shows that, as the point resistance increases the curve first exhibits a positive derivative. There exists a point resistance percentage in which the pile toe residual load ratio to total capacity reaches a maximum value, after which this ratio drops to rising values of point resistance percentage. This maximum occurs, in this case, at 2.7 m penetration, L/D = 16 and toe resistance of 33% of total capacity. For the full penetration, L/D equals 27.4 at a depth of 4.7 m, with a toe resistance percentage of 30% and with a toe residual load reaching 75% of the toe resistance, the maximum mobilization.

Massad reasoned in a personal communication with the author that a similar behavior can also be obtained theoretically by applying his mathematical model conceived for interpreting pile behavior in a load test, Massad (1992, 1993).

8. Conclusions

The residual loads occurring after driving or after the first loading in a static or dynamic pile load test have an important effect on piling behavior (Serviceability Limit State - SLS). Its relevance must be assured especially in piled raft foundations and underpinning designs, where different foundations share the same structural loads. The loads are partitioned according to the different response from each foundation element. In this case an approximate prediction of residual load is essential to obtain a behavior close to the desired serviceability.

When the residual loads are obtained by means of two or more loading cycles in a static load test, it is recommended that the cycles have the same loading rate. This recommendation is especially relevant to clay soils which could exhibit a viscous shear strength with the loading rate (Lopes et al., 2021).

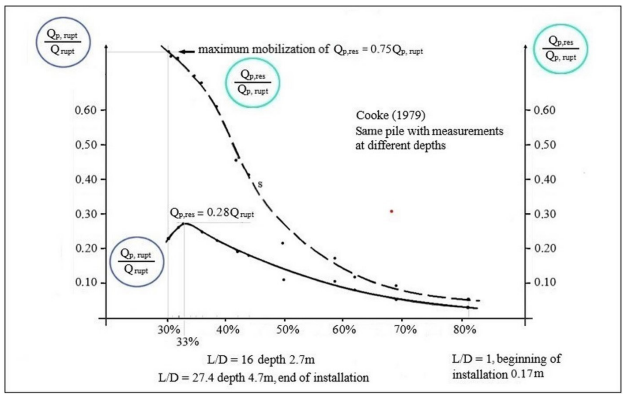

Figure 27. Typical case of piles driven in London clay (data from Cooke, 1979).

The residual shear stresses in soil due to unloading are generated rapidly and might retain a viscous component in plastic soils more susceptible to relaxation effects over time.

The reduction in residual loads after tension load cycling also occurs after compression cycles but resulting in increased residual loads. The final effect concerning the extension of decrease or increase is an issue for future research.

The residual loads affect the settlement prediction of isolated piles. In case of pile groups with pile spacing of three-pile diameters, the effect of residual loads in reducing group settlement is much lower. For a piled raft with greater pile spacing, the reduction of the residual load at pile toe due to the driving neighboring piles is possibly much lower and the effect of residual loads much higher.

The prediction of the residual loads by the wave equation analysis after final stabilized toe displacement is a simple, direct, and accurate procedure with the advantage of including all important factors contributing to residual stresses.

The curves illustrating a first increase and then a decrease of the toe residual load ratio to total capacity versus the point to total capacity percentage were found in stratified, over-consolidated clay and different documented piles in sandy profiles.

In sandy soils the maximum toe residual load to total capacity ratio was found for high point resistance percentage whereas for clayey soils the peak occurred at a much lower percentage.

The ratio of the toe residual load to point resistance, called toe mobilization ratio, revealed a steady downward rate. This curve limits the region of possible curves expressing the ratio of the toe residual load to total capacity ratio and forces the latter's decreasing offset.

Gregersen et al. (1973) results illustrated a high ratio of toe residual load to point resistance for lower stiff pile, and Rieke & Crowser (1987) showed a lower ratio of the toe residual load to point resistance for stiffer piles.

The two curves shown in Figures 22, 26 and 27, expressing the ratio of toe residual load to point resistance

and the ratio of toe residual load to total capacity versus point resistance percentage are similar, respectively, to specific dry soil weight and saturation curve versus water content in soil compaction. The influence of a compaction energy increase in the compaction curve is the same as the pile stiffness reduction in residual toe generated after pile driving or previous pile loading. Furthermore, as the water content increases, the influence of compaction energy in specific dry soil weight tends to decrease. The last comment can also be observed in Figure 26. Although the piles instrumented by Briaud et al. (1989) and Ganju et al. (2020) were stiffer than the piles numerically analyzed by Costa et al. (2001), they were positioned very close to the Costa et al. (2001) curves, unlike the Gregersen et al. (1973) piles. The reduced impact of the stiffness of piles in Briaud et al. (1989) and Ganju et al. (2020) in the proximity to the Costa et al. (2001) curve can be attributed to the high point resistance percentage in the embedded penetration of those piles. This conclusion is the same as the decrease of the influence of compaction energy in specific dry soil weight as the water content increase in a soil sample undergoing compaction.

Acknowledgements

The author is very grateful to the Brazilian Association for Soil Mechanics (ABMS) and honoured for their invitation to present the Pacheco Silva lecture at the 20th Brazilian Conference on Soil Mechanics and Geotechnical Engineering in Campinas (SP) in August 2022. The author also expresses her gratitude to Kessylyn Nogueira Ramos for her valuable support in preparing the figures in the article.

Declaration of interest

The author has no conflicts of interest to declare.

Data availability

No dataset was generated or evaluated in the course of the current study; therefore, data sharing is not applicable.

List of symbols

a_r Residual load ratio at pile toe to pile point capacity in percentage
d Pile diameter
m Ratio of shaft resistance to total pile resistance in percentage
E_P Young's pile modulus
E_s Soil Young modulus
$f_{s,rupt}$ The pile soil friction on pile shaft available at failure
K_p Pile and soil relative stiffness at the pile toe
K_τ' Pile and soil relative stiffness at the pile lateral surface
L Pile embedded length
N_v The variation of Young's modulus of soil with depth
P Load applied at pile top
$Q_{l,\ measured}$ Load difference between measurement at pile top and toe
$Q_{l,\ measured}$ (F) Load difference between measurement at pile top and toe at failure when instruments are zeroed before the test, false value.
$Q_{l,\ rupt}$ Pile lateral bearing capacity
$Q_{l,\ rupt}$ (T) True pile lateral bearing capacity (the same as $Q_{l,\ rupt}$) $Q_{max,\ res}$ Maximum residual load at the neutral plane
$Q_{p,\ measured}$ Load measured at pile toe
$Q_{p,mobilized}$ Resistance mobilized at pile toe
$Q_{p,\ res}$ Residual load at pile toe
$Q_{p,\ rupt}$ Pile point bearing capacity
$Q_{rebound}$ Load corresponding to the recoverable settlement
Q_{rupt} Pile total bearing capacity
$Q_{t,mobilized}$ Total mobilized resistance in a load test
$Q_{t,2}$ Maximum total load in the second loading of a pile load test
$Q_{z,res}$ Residual load at depth z
β Rate of increase of shaft friction with depth
$\delta_{rebound}$ Recoverable settlement of the second loading of the load test

References

Briaud, J., & Tucker, L. (1984). Piles in sand: a method including residual stresses. *Journal of Geotechnical Engineering*, 110(11), 1666-1680. http://dx.doi.org/10.1061/(ASCE)0733-9410(1984)110:11(1666).

Briaud, J., Tucker, L., & Ng, E. (1989). Axially loaded 5 pile group and single pile in sand. In *Proceedings of the 12th International Conference on Soil Mechanics and Foundation Engineering* (Vol. 2, pp. 1121-1124). Rotterdam: Balkema.

Cooke, R.W. (1979). Influence of residual installation forces on the stress transfer and settlement under working loads of jacked and bored piles in cohesive soils. In *Symposium on Behavior of Deep Foundation* (Publication STP 670, pp. 231-249). West Conshohocken: ASTM.

Cooke, R.W., & Price, G. (1973). Strains and displacements around friction piles. In *Proceedings of the 8th Conference on Soil Mechanics and Foundation Engineering* (Vol. 2, pp. 53-60). Moscow: SIMSG ISSMGE.

Costa, A. M. (1988). *DINEXP Manual*. PETROBRÁS Internal Report. (in Portuguese).

Costa, L.M., Danziger, B.R., & Lopes, F.R. (2001). Prediction of residual driving stresses in piles. *Canadian Geotechnical Journal*, 38(2), 410-421. http://dx.doi.org/10.1139/t00-095.

Danziger, B.R., & Lopes, F.R. (2008). Discussion of development of residual forces in long driven piles in weathered soils. *Journal of Geotechnical and Geoenvironmental*

Engineering, 134(10), 1420-1421. http://dx.doi.org/10.1061/(ASCE)1090-0241(2008)134:9(1420).

Danziger, B.R., Costa, A.M., Lopes, F.R., & Pacheco, M.P. (1992). Back-analyses of closed-end pipe piles for an offshore platform. In *Proceedings of the 4th International Conference on the Application of Stress Wave Theory to Piles* (Vol. 1, pp. 557-562). Rotterdam: Balkema.

Danziger, B.R., Costa, A.M., Lopes, F.R., & Pacheco, M.P. (1999). Back-analyses of offshore pile driving with an improved soil model. *Geotechnique*, 49(6), 777-799. http://dx.doi.org/10.1680/geot.1999.49.6.777.

Darrag, A.A., & Lovell, C.W. (1989). A simplified procedure for predicting residual stresses for piles In *12th International Conference on Soil Mechanics & Foundation Engineering* (pp. 1127-1130). Rotterdam: Balkema.

Decourt, L. (1989). Instrumented bored piles in residual soils. In *12th International Conference on Soil Mechanics and Foundation Engineering.* Rotterdam: Balkema.

Decourt, L. (1991). Thoughts concerning the interpretation of successive load tests on the same pile. In *9th Panamerican Conference on Soil Mechanics and Foundation Engineering* (Vol. 2, pp.585-597). Santiago: Sociedad Chilena de Geotecnia.

Decourt, L., & Quaresma, A.R. (1978). Capacidade de carga de estacas a partir de valores de SPT. In *6th Congresso Brasileiro de Mecânica dos Solos e Engenharia de Fundações* (Vol. 1, pp. 45-53). São Paulo: ABMS.

Fellenius, B.H. (2002). Determining the residual distribution in piles. Part 2: method for determining the residual load. *Geotechnical News Magazine*, 20(3), 25-29.

Fellenius, B.H. (2023). *Basics of foundation design*. Lulu.

Fonseca, A.V., Santos, J.A., Esteves, E.C., & Massad, F. (2007). Analysis of piles in residual soil from granite considering residual loads. *Soils & Rocks*, 30(2), 63-80. http://dx.doi.org/10.28927/SR301063.

Ganju, E., Han, F., Prezzi, M., & Salgado, R. (2020). Static capacity of closed-ended pipe pile driven in gravelly sand. *Journal of Soil Mechanics and Environmental Engineering*, 146(4), http://dx.doi.org/10.1061/(ASCE)GT.1943-5606.0002215.

Goble, G.G., & Hery, P. (1984). Influence of residual forces on pile driveability. In *Proceedings of the 2nd International Conference on the Application of Stress Wave Theory to Piles* (pp. 154-161). Stockholm: Swedish Pile Commission.

Goble, G.G., Rausche, F., & Likins, G.E. (1988). *GRLWEAP program: wave equation analysis of pile driving: procedures and models – program manual*. Pile Dynamics Inc.

Gregersen, O.G., Aas, G., & DiBiagio, E. (1973). Load tests on friction piles in loose sand. In *8th International Conference on Soil Mechanics and Foundation Engineering* (pp. 109-117). Moscow: SIMSG ISSMGE.

Hery, P. (1983). *Residual stress analyses in WEAP* [Doctoral thesis]. University of Colorado.

Holloway, D.M., Clough, G.W., & Vesic, A.S. (1978). The effects of residual driving stress on piles performance under axial loads. In *Proceedings of Offshore Technology Conference* (pp. 2225-2236). New York: American Society of Mechanical Engineers.

Hunter, A.H., & Davisson, M.T. (1969). Measurement of pile load transfer. In R. Lundgren & E. D'Appolonia (Eds.), *Performance of deep foundation* (Special Technical Publication, pp. 106-117). ASTM.

Kim, S.R., Chung, S.G., & Fellenius, B.H. (2011). Distribution of residual load and true shaft resistance for a driven instrumented test pile. *Canadian Geotechnical Journal*, 48(4), 583-598. http://dx.doi.org/10.1139/t10-084.

Kou, H.L., Chu, J., Guo, W., & Zhang, M.Y. (2016). Field study of residual forces developed in pre-stressed high-strength concrete (PHC) pipe piles. *Canadian Geotechnical Journal*, 53(4), 696-707. http://dx.doi.org/10.1139/cgj-2015-0177.

Liu, M., & Zhang, M. (2012). Measurement of residual force locked in open-ended pipe pile using FBG-based sensors. *The Electronic Journal of Geotechnical Engineering*, 17, 2145-2154.

Liyanapathirana, D.S., Deeks, A.J., & Randolph, M.F. (1998). Numerical analysis of soil plug behavior inside open-ended piles during driving. *International Journal for Numerical and Analytical Methods in Geomechanics*, 22(4), 303-322. http://dx.doi.org/10.1002/(SICI)1096-9853(199804)22:4<303:AID-NAG919>3.0.CO;2-P.

Liyanapathirana, D.S., Deeks, A.J., & Randolph, M.F. (2000). Numerical modelling of large deformations associated with driving of open-ended piles. *International Journal for Numerical and Analytical Methods in Geomechanics*, 24(14), 1079-1101. http://dx.doi.org/10.1002/1096-9853(20001210)24:14<1079:AID-NAG113>3.0.CO;2-E.

Lopes, F.R., Santa Maria, P.E.L., Danziger, F.A.B., Martins, I.S.M., Danziger, B.R., & Tassi, M.C. (2021). A proposal for static load test in piles: the equilibrium method. *Soils & Rocks*, 44(1), 1-10. http://dx.doi.org/10.28927/SR.2021.057920.

Marques, J.A.F., & Massad, F. (2004). Provas de carga instrumentadas em estacas escavadas com bulbos, executadas na Região Praieira de Maceió, Alagoas. *Solos e Rochas*, 2(3), 243-260.

Mascarucci, Y., Mandolini, A., & Miliziano, S. (2013). Effects of residual stresses on shaft friction of bored cast in situ piles in sand. *Journal of Geo-engineering Sciences*, 1, 37-51. http://dx.doi.org/10.3233/JGS-13009.

Massad, F. (1992). Sobre a interpretação de provas de cargas em estacas considerando as cargas residuais na ponta e a reversão do atrito lateral. Parte I: solos relativamente homogêneos. *Solos e Rochas*, 15(2), 103-115.

Massad, F. (1993). Sobre a interpretação de provas de cargas em estacas considerando as cargas residuais na ponta e a reversão do atrito lateral. Parte II: estaca embutida em solo mais resistente. *Solos e Rochas*, 16(2), 93-112.

Massad, F. (1995). The analysis of piles considering soil stiffness and residual stresses. In *10th Panamerican*

Conference on Soil Mechanics and Foundation Engineering (Vol. 2, pp. 1199-1210). Mexico: Sociedad Mexicana de Mecánica de Suelos.

Massad, F. (2001). On the use of elastic rebound to predict pile capacity. In *15th International Conference on Soil Mechanics on Soil Mechanics and Geotechnical Engineering* (Vol. 2, pp. 1199-1210). Istanbul: Maya.

Massad, F., & Lazo, G. (1998). Graphical method for the interpretation of the load-settlement curve from vertical load tests on rigid and short piles. In *11 Congresso Brasileiro de Mecânica dos Solos e Engenharia Geotécnica* (Vol. 3, pp. 1407-1414). Brasília, DF: ABMS.

Mussara, M., & Massad, F. (2015). Static load tests in an instrumented rock socket barrete pile. *Soils & Rocks*, 38(2), 163-177. http://dx.doi.org/10.28927/SR382163.

Nie, R., Leng, W., Wu, A., Li, F., & Chen, Y.F. (2014). Field measurement and analysis of residual stress in bored piles. *Journal of Highway and Transportation Research and Development*, 8(4), 57-62. http://dx.doi.org/10.1061/JHTRCQ.0000411.

Poulos, H. (1987). Analysis of residual stress effects in piles. *Journal of Geotechnical Engineering*, 113(3), 216-229. http://dx.doi.org/10.1061/(ASCE)0733-9410(1987)113:3(216).

Poulos, H., & Davis, E.H. (1980). *Pile foundation analysis and design*. John Wiley & Sons.

Randolph, M.F. (1991). The effect of residual stress in interpreting stress wave data. *Computer Methods and Advances in Geomechanic*, 1, 777-782.

Rausche, F., Richardson, B., & Likins, G. (1996). Multiple blow CAPWAP analysis of pile dynamic records. In *Proceedings of the 5th International Conference on the Application of Stress Wave Theory to Pile* (Vol. 1, pp. 435-446). Rotterdam: Balkema.

Rieke, R.D., & Crowser, J.C. (1987). Interpretation of pile load test considering residual stresses. *Journal of Geotechnical Engineering*, 113(4), 320-334. http://dx.doi.org/10.1061/(ASCE)0733-9410(1987)113:4(320).

Smith, E.A.L. (1960). Pile driving analysis by the wave equation. *Journal of the Soil Mechanics and Foundations Division*, 86(4), 35-61. http://dx.doi.org/10.1061/JSFEAQ.0000281.

Vesic, A.S. (1977). On the significance of residual loads for response of piles. In *9th International Conference on Soil Mechanics and Foundation Engineering* (Vol. 3, pp. 374-379). Tokyo: ICSMFE.

Zhang, L.M., & Wang, H. (2007). Development of residual forces in long driven piles in weathered soils. *Journal of Geotechnical and Geoenvironmental Engineering*, 133(10), 1216-1228. http://dx.doi.org/10.1061/(ASCE)1090-0241(2007)133:10(1216).